10.1098/rspa.2003.1219

THE ROYAL SOCIETY

Does the low frequency variability of mesoscale dynamics explain a part of the phytoplankton and zooplankton spectral variability?

By Marina Lévy[1] and Patrice Klein[2]

[1]*LODYC/IPSL, Université Pierre et Marie Curie, 4 place Jussieu, 75252 Paris CEDEX 05, France* (marina.levy@lodyc.jussieu.fr)
[2]*LPO, IFREMER, BP 70, 29280 Plouzane, France* (patrice.klein@ifremer.fr)

Received 1 April 2003; accepted 18 July 2003; published online 16 March 2004

Observational studies of the last 20 years have revealed a spatial distribution of phytoplankton characterized by a wavenumber spectrum whose slope ranges between k^{-1} and k^{-3} (with k being the wavenumber), over horizontal scales ranging from 10 to 100 km. This strong spectral variability can be due either to the physics and/or to the biology. We show in this note that the low frequency variability (LFV) linked to the mesoscale dynamics may explain a significant part of the observed variability. Our numerical results also suggest that the difference between the phytoplankton and zooplankton spectral slopes can depend on the dynamical LFV.

Keywords: plankton patchiness; mesoscale eddies; spectral variability

1. Introduction

The wavenumber spectrum of any dynamical quantity in the upper oceanic layers is known to display a spectral peak at *ca.* 100 or 200 km (Stammer 1997; Wunsch 1997; Smith & Vallis 2001), which corresponds to the scale of the energetic mesoscale eddies that populate all the oceans. Between this peak and a scale of 10 km, these spectra are usually characterized by a power law of the form k^{-n}, with n varying, for example, from 4 or 3 for the kinetic energy to 3 or 2 for the sea-surface temperature. The value n characterizes the spatial distribution of the quantity examined, since it indicates whether the small-scale structures are energetic (small n) or not (large n) relative to the structures of larger scales. The rationalization of this power law mostly involves the horizontal stirring (or deformation) processes induced by energetic eddies (Tennekes & Lumley 1972). These stirring processes, intensively studied these last ten years in terms of chaotic advection (Lapeyre *et al.* 1999), are governed principally by the mesoscale velocity field (Klein & Hua 1990). The result is the direct cascade that transforms large-scale patterns of any passive tracer into small-scale filaments. When it comes to a purely passive tracer (i.e. one that has no feedback on the dynamical field, and that is not submitted to source–sink processes), theoretical arguments of two-dimensional (2D) turbulence show that, at equilibrium, the spectrum of such a tracer has a slope of k^{-1} (Kraichnan 1974). This is *not* what is observed for phytoplankton. Furthermore, the phytoplankton spectrum

slope is not universal, since values ranging from k^{-1} to k^{-3} have been reported, from ship transects and sea-colour images (Gower *et al.* 1980; Smith *et al.* 1988; Yoder *et al.* 1993; Strutton *et al.* 1997; Washburn *et al.* 1998; Martin & Srokosz 2002). Thus, a phytoplankton field may involve more- or less-energetic small-scale structures. Since Gower *et al.* (1980), a serious debate has developed to try to understand the additional role of the biological factors in explaining the observed phytoplankton and zooplankton spectra (as illustrated by the studies of Powell & Okubo (1994), Smith *et al.* (1996), Abraham (1998), Lévy *et al.* (2001*a*), Martin & Srokosz (2002), Martin *et al.* (2002) and Mahadevan & Campbell (2002)). A possible effect of biological activity has been elegantly described and rationalized by Abraham (1998). His scenario involves nitrates injected at large scales and the resulting production of phytoplankton and zooplankton, the three of them being stirred by a turbulent eddy field. Because of rapid consumption by phytoplankton, the nitrates have no time to be fully stirred into energetic small scales and therefore the resulting nitrate cascade has no time to equilibrate. The same behaviour holds for phytoplankton because of grazing by zooplankton. Hence nitrate has a steeper spectrum slope than phytoplankton, which has a steeper spectrum slope than zooplankton. Abraham & Bowen (2002) propose a simple theoretical explanation for the resulting slope values in terms of a ratio involving the biological rates and the Lyapunov exponents (which express the exponential character of the effects due to the stirring processes). Hence different biological rates could lead to different spectrum-slope values.

However, even if these biological factors can play a role in plankton spectral variability, it is primarily the dynamics, and mostly the mesoscale stirring processes, that drive the plankton spatial distribution (Abraham *et al.* 2000). Within this context there is a dynamical characteristic, rarely considered in the studies mentioned previously, that can be invoked: the fact that the statistical properties of mesoscale turbulence significantly vary with time. Indeed numerous 'dynamical' studies have displayed and rationalized the low frequency variability (LFV) (at scales between 10 days and more than 100 days) of the eddy kinetic energy (EKE) and its resulting impact on the variability of the spectrum-slope values. The essence of this LFV, revealed by earlier geophysical studies (see Pedlosky & Frenzen 1980), relies principally on the nonlinear interactions between the eddy field and the mean flow. Later studies have put forward the importance of this LFV to explain the persistence and changes of the weather regimes in the atmosphere (Ghil & Childress 1987; Vautard & Legras 1988). The thorough study by Panetta (1993) shows that this LFV exists in a large region of the parameter space including that of the ocean dynamics, which was confirmed, for example, in the Antarctic circumpolar current by Tréguier & Panetta (1994). Temporal changes in eddy energy of the oceans (Stammer & Wunsch 1999; Penduff *et al.* 2004), diagnosed from satellite altimeter observations, show LFV in large regions of the ocean. The time-scales involved (more than 10 days) are larger than those associated with the biological variables so we expect a decoupling between the effects of biological processes and dynamical processes, which would emphasize the importance of the latter at these scales. Then, to extend the ongoing debate, we postulate in the present study that the time variability of the mesoscale eddy field contributes to the spectral variability of the plankton distribution.

More precisely, an experimental protocol has been designed to address the question: does the LFV associated with the mesoscale turbulence explain a part of the plankton spectral variability? This protocol involves a numerical turbulent eddy field

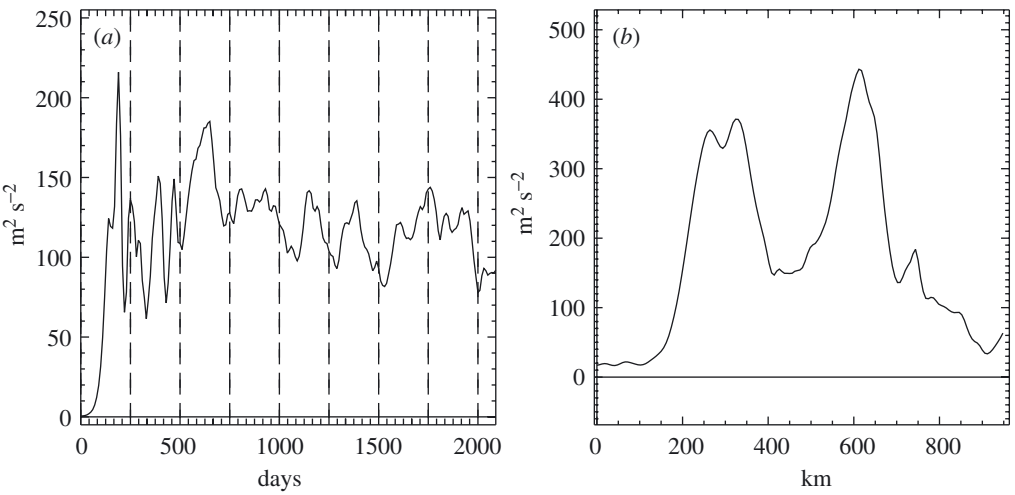

Figure 1. Time evolution of (*a*) the surface turbulent (eddy) kinetic energy (TKE, with respect to a zonal average) and (*b*) the meridional distribution (zonal average) of the surface TKE at day 2000.

and a basic biological model. The very simple design of our experiments only allows us to illustrate that the physics *can* explain a large part of the observed spectral variability of plankton, *not* that it always does. Our experiments are, however, more complex than those previously conducted (Abraham 1998; Martin *et al*. 2002): they involve a small-scale vertical injection of nutrients intimately organized by the eddy field, instead of a large-scale injection of nutrients (Abraham 1998) or an arbitrarily distributed small-scale injection (Martin *et al*. 2002). These experiments are thus fully three dimensional (3D) instead of quasi-bidimensional. Section 2 presents the protocol used, §§ 3 and 4 discuss the numerical results, and conclusions are offered in § 5.

2. The experimental protocol

The time evolution of a turbulent eddy field is simulated in a zonally periodic β-plane channel (1300 km and 960 km, respectively, in the zonal and meridional direction) with a primitive equation ocean model (Madec *et al*. 1998). The eddy field results from the instability of a zonal baroclinic current. After a spin-up period of *ca*. 500 days, eddies permanently exchange energy with the mean flow, which causes the EKE in the upper layers to fluctuate in time (figure 1). After an adjustment period of 1600 days for the dynamics, the full physical–biological system is run for 500 days, with outputs every 10 days. The biological model is based on nitrogen (cf. Fasham *et al*. 1990), and describes the interactions between nitrate, phytoplankton, zooplankton, ammonium, detritus and dissolved organic matter (Foujols *et al*. 2000; Lévy *et al*. 2001*a*). The model simulates an oligotrophic regime perturbed by the fertilizing action of a weakly energetic eddy field, as can be encountered in the centre of sub-tropical gyres. The flow impacts on the ecosystem through the horizontal and vertical advection of the six biological variables, which are considered as tracers subjected to biological interactions between them. The main nitrogen source is nitrate, which is injected into the euphotic layer through eddy-induced vertical advection.

To assess the specific role of the biological interactions, a passive tracer, initialized with uniform values of zero above and one below 100 m in order to mimic the nitrate vertical gradient, was also considered. Therefore, the spatial heterogeneity of this passive tracer is entirely set up by the dynamical processes, with vertical advection acting as a source for the upper 100 m, and horizontal advection as a horizontal redistribution. The characteristics of the physical and biological models, as well as those of the numerical simulations performed, are detailed in the appendix.

As expected, the time evolution of the surface EKE during the spin-up period (figure 1) is significant: after a transitory period of *ca.* 500 days, EKE fluctuates with time-scales from 30 to 300 days and amplitude variations of up to 50%. At times, two zonal jets dominate the eddy field (figure 1), whereas eddies strongly dominate at other times. The intermittent appearance of these zonal jets is of course intimately related to the amplitude of the EKE relative to the mean-flow kinetic energy. This spatial distribution is a common feature of the nonlinear response of unstable baroclinic jets (Panetta 1993). The next two paragraphs examine at a given time the characteristics (in physical and spectral spaces) of the dynamical and biological variables.

(*a*) *Snapshots of the turbulent eddy field*

The snapshots at day 1970 of the relative-vorticity and temperature (or density) fields at the surface (figure 2) reveal mesoscale eddies with scales between 50 and 150 km. Relative vorticity values range from $-0.4f$ to $0.7f$ (where f is the Coriolis frequency). Temperature variations are of the order of 10% of the mean value. Small-scale structures in the relative-vorticity field appear to be more energetic than those in the temperature field.

In order to quantitatively compare the contribution of the various space scales with the total variance of each field, we applied a 2D fast Fourier transform to the variance of these images. We formed auto spectra as functions of a scalar wavenumber. We obtained an equivalent one-dimensional (1D) spectrum by summing spectral coefficients in concentric rings in 2D wavenumber space, thereby conserving variance. Spectra of the preceding dynamical fields (figure 3) exhibit a peak at wavenumber $k = 7$ (corresponding to 137 km) and a power-law form between $k = 7$ and $k = 60$ (corresponding to 16 km). The peak (at 137 km) roughly corresponds to the scale of the energetic eddies. For wavenumbers greater than 60, the variance strongly decreases due to the selective small-scale dissipation associated with the biharmonic operator. In the range 16–137 km, the relative-vorticity spectrum displays a slope of $k^{-1.1}$ and the temperature spectrum a slope of $k^{-2.77}$.

These values are consistent with results of mesoscale turbulence studies near the surface (Held *et al.* 1995). The explanation for the steep slope of the temperature (or density) spectrum (see Klein *et al.* 1998) is that the 3D advection mechanisms are organized so as to prevent the formation of energetic small scales of temperature (which would strongly increase the thermal-wind imbalance and thus produce a dynamical inconsistency). In other words, there is a phase relationship between horizontal and vertical velocities such that the contributions of the vertical advection and of the horizontal advection of temperature strongly compensate each other. This process is the explanation of how the direct cascade of temperature (or density) is inhibited. However, this compensation does not pertain to quantities (such as

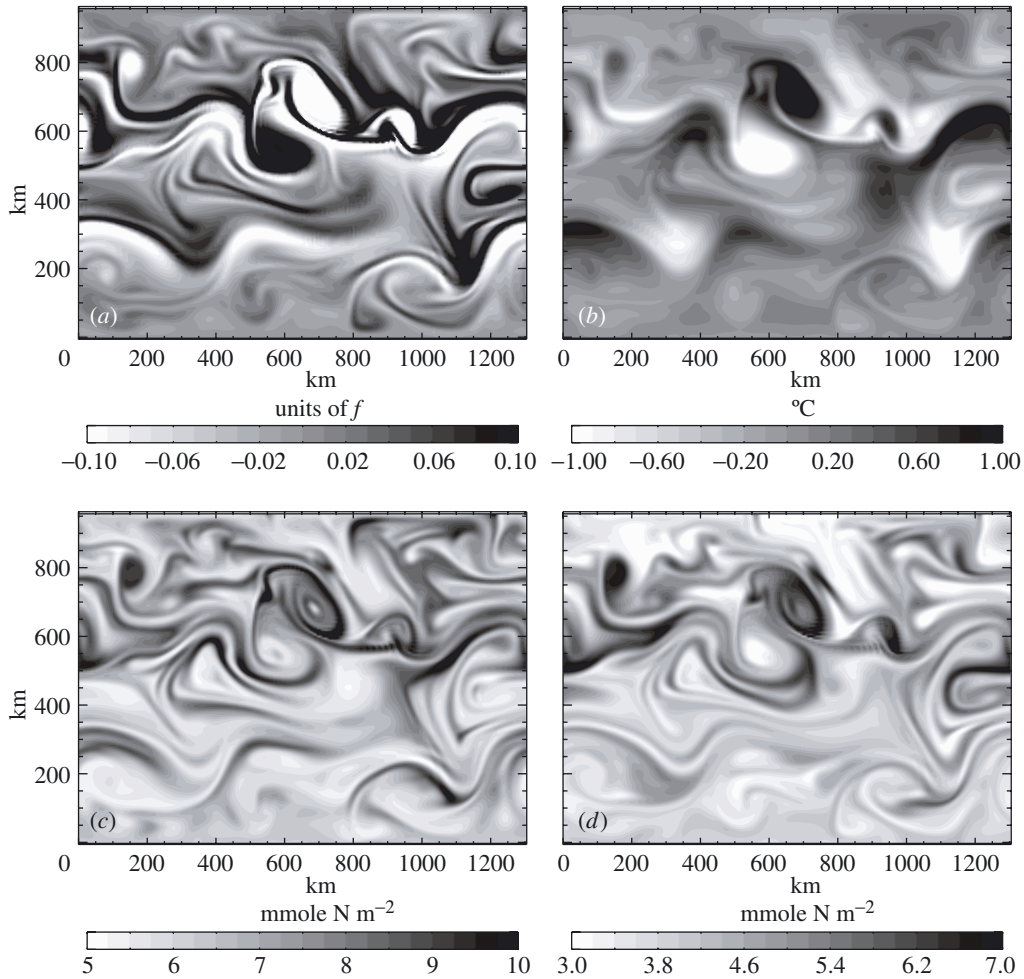

Figure 2. Snapshots at day 1970 of (*a*) surface relative vorticity, (*b*) surface-temperature anomaly (with respect to the zonal mean), (*c*) 0–150 m phytoplankton and (*d*) 0–150 m zooplankton.

relative vorticity or any passive tracer) whose initial conditions (and forcing terms) differ from those of temperature. In that case, the direct cascade from large to small scales is efficient, and produces energetic small scales.

(*b*) *Snapshots of the plankton fields*

Figure 2 displays a snapshot at day 1970 of the phytoplankton and zooplankton fields, integrated from the surface down to 150 m. Indeed, a characteristic of the oligotrophic regime is that plankton maxima remain at sub-surface, and at a depth that varies with the intensity of the nitrate injection. Therefore, in order to focus on the horizontal patchiness, our analyses are performed on vertically integrated plankton fields over the top 150 m.

The ratio between the minimum and maximum phytoplankton concentrations is of the order of three. The same ratio is found for zooplankton. The plankton fields have spatial characteristics much closer to those of relative vorticity than to those

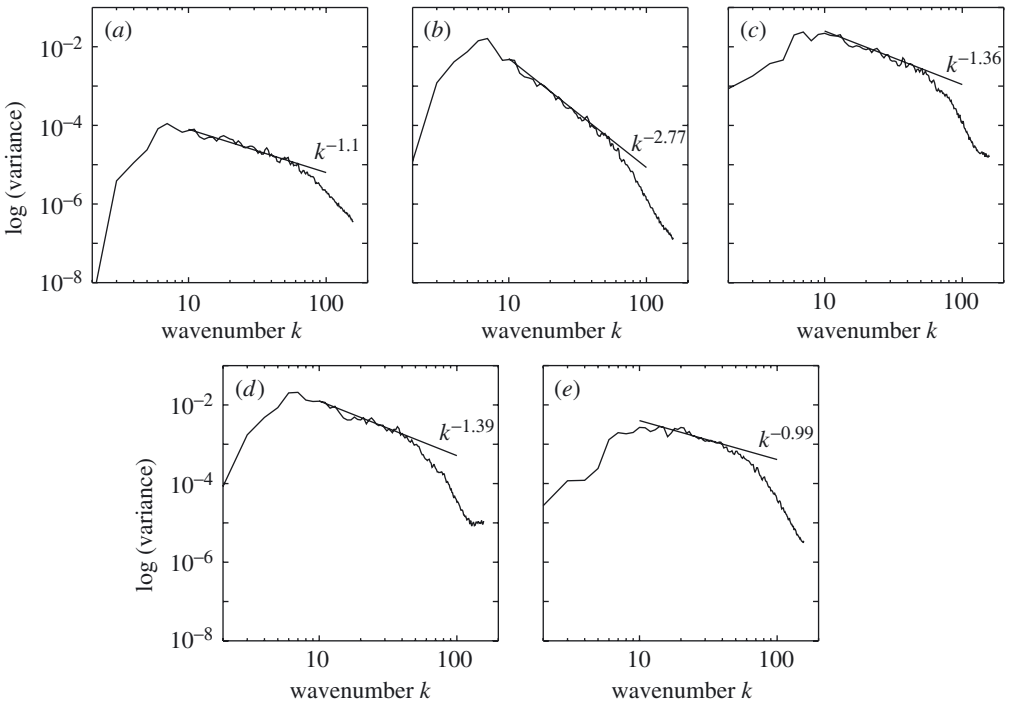

Figure 3. Variance spectra of the fields displayed in figure 2 ((*a*) surface relative vorticity, (*b*) temperature, (*c*) 0–150 m phytoplankton and (*d*) 0–150 m zooplankton) and of (*e*) a passive tracer (integrated over 0–150 m). Slopes, estimated from linear regressions between wavenumbers 8 and 50, are also drawn.

of temperature. Qualitatively, figure 2 shows that plankton and relative-vorticity fields exhibit energetic sub-mesoscale features at the same locations. A quantitative analysis of that correspondence in the next paragraph will also reveal that the phase of the small-scale structures in plankton and vorticity are coherent, with plankton being more abundant in negative-vorticity filamentary structures.

Plankton and passive-tracer spectra (figure 3) exhibit a peak at the same wavenumber as that for the dynamical variables (i.e. at $k = 7$). The passive-tracer field (also integrated between 0 and 150 m) displays a spectrum slope close to the theoretical value ($k^{-0.99}$). The biological spectrum slopes differ slightly from those of the relative vorticity and of the passive-tracer fields: phytoplankton has a $k^{-1.36}$ slope and zooplankton a $k^{-1.39}$ slope. As Abraham's (1998) experiments suggest, these values are likely to be sensitive to the biological rates. One now has to address the question of this study, i.e. whether these plankton spectrum slopes are steady in time and, if not, what makes them vary (since, in our simulation, biological rates are constant). An examination of the time-series of the different variables over 500 days, given in § 3, will provide an answer to this question.

3. Results over 500 days

The 500 days of the simulation (after the adjustment period of 1600 days) reveal that the preceding spectral characteristics of the dynamical and biological fields are

Table 1. *Statistics on spectral slopes*

(For relative vorticity and temperature, slopes are computed from surface fields. For phytoplankton, zooplankton and the passive tracer, the slopes are computed on the 0–150 m integrated fields. For each field, 50 snapshots are available, and spectral analysis is performed on each snapshot. The mean slope is the mean respective to the ensemble of snapshots. The standard deviation is respective to that of the mean. The minimum and maximum are the extremum slope values obtained among the 50 snapshots.)

	mean	maximum	minimum	standard deviation
relative vorticity	−1.64	−1.2	−2.1	0.15
temperature	−3.17	−2.8	−3.5	0.15
phytoplankton	−1.50	−1.2	−1.7	0.11
zooplankton	−1.65	−1.2	−2.1	0.18
passive tracer	−1.42	−1.0	−1.7	0.17

not steady. Instead, they strongly vary with time. Furthermore, they show that the time variability of plankton spatial distribution is mostly driven by the dynamical fields. A persistent signature of this *dynamical guidance* is the strong resemblance, in physical space, between plankton and relative-vorticity patterns: at any time during these 500 days, phytoplankton and zooplankton concentrations are mostly enhanced in negative-vorticity structures.

(*a*) *Spectral characteristics*

The time variability of the patchiness of physical and biological variables is assessed by calculating the corresponding spectra for each of the 50 available snapshots (one every 10 days for 500 days). Consistent with the results for the EKE (figure 1), spectrum slopes reveal a significant LFV (figure 4). As before, the spectrum slopes are computed by applying linear regressions between wavenumbers 10 and 50. Remarkably, the standard deviation on the linear regressions never exceeds 5% although the values of the spectral slopes show strong temporal variation. Moreover, we evaluate the absolute error in the computation of the slope due to the choice of the wavenumber range (in the larger limit $k = 7$ to $k = 60$) to be ± 0.1. The relative results (comparison between slopes of different variables) do not depend on the exact choice of the wavenumber range, provided that the same range is used for all variables.

The mean spectral slope (over 500 days) for surface relative vorticity is −1.64, but the extremum values are −1.2 and −2.1, with a standard deviation of 0.15 (see table 1). The mean passive tracer spectrum slope (−1.42) is flatter than the mean relative vorticity spectrum slope. The phytoplankton spectrum slope lies between the two: its range is between −1.2 and −1.7 with a mean value of −1.5. The temperature spectrum slope is of course much steeper and ranges between −2.8 and −3.5 with a mean value of −3.17. These values are consistent with observations (see, for example, Martin & Srokosz 2002).

Relative vorticity, temperature, phytoplankton and passive tracer spectral slopes show LFV (figure 4) on time-scales of the order of 30–100 days (the case for zooplankton is discussed later). A very important peculiarity is that the phase of this variability is about the same for all biological and dynamical fields. Except for zooplankton,

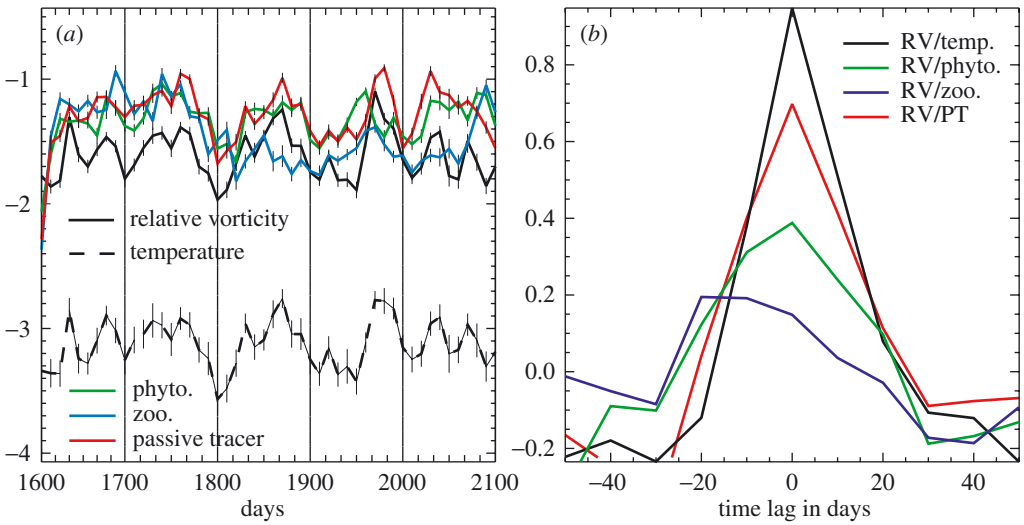

Figure 4. (*a*) Time evolution of the spectrum slopes of surface relative vorticity, temperature, 0–150 m phytoplankton, 0–150 m zooplankton and passive tracer. The slopes are computed using a linear regression between wavenumbers 10 and 50. The error bars account for the standard deviation. (*b*) Cross-correlations between the slope time-series: slopes of relative vorticity versus slopes of temperature, phytoplankton and zooplankton.

the peak correlation between the time-series of the relative vorticity spectrum slope and the slopes of other variables occurs at zero lag (figure 4), indicating that the patterns evolve simultaneously (or at least within a lag shorter than 10 days). The cross-correlation of the zooplankton and vorticity spectrum slopes is maximum at a lag of 20 days, mirroring the expected lag of zooplankton growth to recently upwelled nutrients. The peak correlation is higher (0.7) for the passive tracer than for phytoplankton (0.4). This may reflect the additional role of the biological factors, and/or that of the peculiar vertical variability that characterizes the plankton distribution in oligotrophic regimes (see the appendix).

Our present time-series is not long enough to determine which specific frequencies emerge, and to analyse more precisely the phase lag between the variables. However, these results clearly suggest that the LFV of plankton is strongly driven by that of the dynamical fields. In addition, since both relative vorticity and plankton exhibit energetic small-scale structures, the remarkable phase relationship of the evolution of their spectral slopes indicates that the time evolution of the variance associated with the small-scale plankton patterns closely follows that of the small-scale vorticity structures.

The spectral slope for zooplankton shows an additional variability on longer time-scales (300 days), which our time-series does not allow us to address in detail. This variability on longer time-scales is likely to be driven by the interaction between mesoscale and biological dynamics. It causes a loss of correlation between the time variability of the relative-vorticity and zooplankton spectral slopes (figure 4). As a result, at times (such as during the first 150 days), zooplankton spectra are flatter than phytoplankton spectra, but at other times they are steeper. Discussions in Abraham (1998) and Martin & Srokosz (2002) emphasized that spectral slopes of phytoplankton and zooplankton can significantly depend on the biological rates.

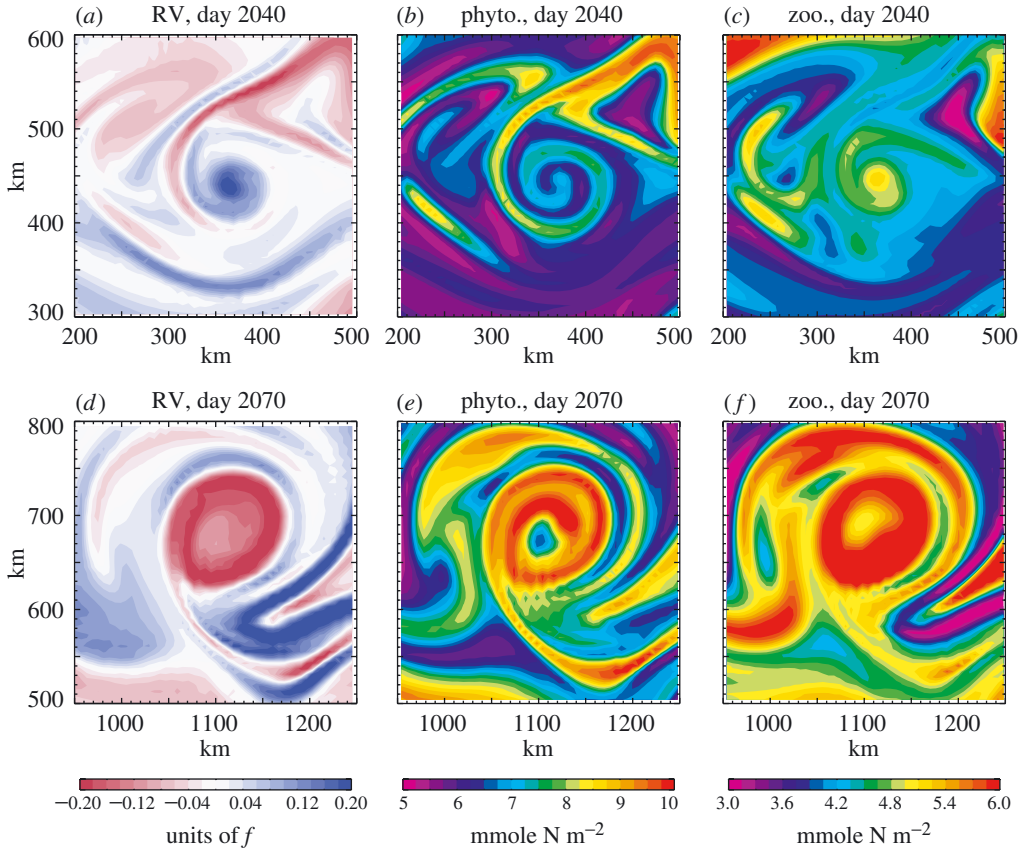

Figure 5. Relative vorticity, 0–150 m phytoplankton and 0–150 m zooplankton within (*a*)–(*c*) a cyclone and (*d*)–(*f*) an anticyclone. The figure parts show snapshots at days 2040 and 2070.

One cannot invoke here biological dynamics to explain the differences between the phytoplankton and zooplankton spectra, since biological rates are constant. These results suggest that the difference between the phytoplankton and zooplankton spectral slopes may depend on dynamically driven LFV.

(*b*) *Relationship between mesoscale dynamics and biology in physical space*

The spectral analysis clearly illustrates that the time variability of the plankton patchiness is strongly driven and constrained by the time-varying spatial distribution of the turbulent eddy field, which involves both mesoscale and sub-mesoscale dynamical structures. Furthermore, as seen in figure 2 and in a large number of subsequent snapshots (not shown), phytoplankton and zooplankton appear to be associated with the relative-vorticity patterns: plankton is more abundant in negative-vorticity regions and less abundant in positive-vorticity regions. This is all the more apparent in figure 5, which shows the relative vorticity, phytoplankton and zooplankton in the neighbourhood of two specific structures: a cyclonic and an anticyclonic eddy. The cyclone is surrounded by a negative-vorticity filament. Phytoplankton concentration appears to be particularly enhanced within this filament and in other adjacent

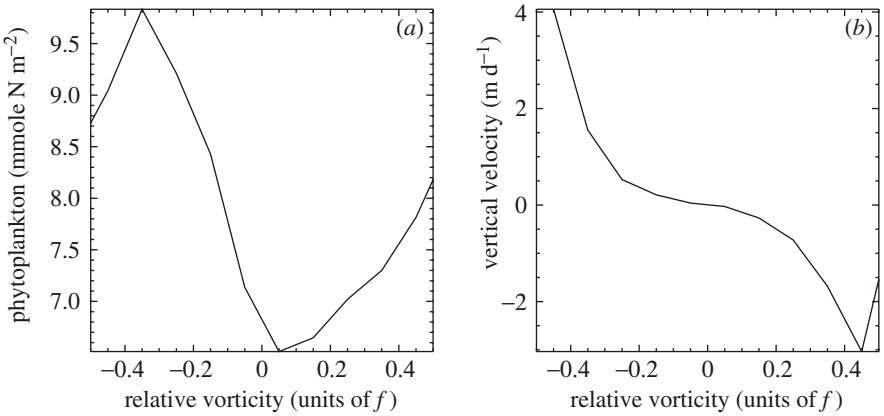

Figure 6. Plots of (*a*) phytoplankton (0–150 m) and (*b*) vertical velocities (at 100 m) versus relative vorticity. Values represent averages over vorticity bins of width $0.1f$. Data from the 500 days of the run are considered.

negative-vorticity filaments. On the contrary it is depleted in positive-vorticity filaments. Zooplankton is globally enhanced where phytoplankton is enhanced, but is not correlated with phytoplankton within the small-scale spiral. It is enhanced within the cyclone. The phytoplankton concentration is enhanced at the inner border of the anticyclone, where negative relative vorticity is at a maximum. The resulting pattern is a ring of phytoplankton. In this eddy, zooplankton patterns closely resemble the phytoplankton patterns.

This relationship between vorticity and phytoplankton is statistically found at any time in the simulation. As a result, the mean (over the entire time-series) correlation between phytoplankton and vorticity is -0.41, with a standard deviation of 0.05. It is slightly smaller than the correlation between new production and vorticity (-0.47 on average). Both are related to the high correlation between nitrate and vorticity just below the euphotic layer (-0.73 on average). The correlation between phytoplankton and zooplankton is also high: 0.53 on average. Another way to diagnose the relationship between phytoplankton and vorticity is to calculate at each model grid point the correlation between the time-series of the two fields. The resulting correlation field (not shown) is found to be negative over most of the domain (96%), which confirms the parity between phytoplankton and vorticity. Over 45% of the domain, the correlation is higher than -0.5 and it is higher than -0.4 over 63% of the domain. The highest correlation reached is -0.9. A student test shows that phytoplankton and vorticity are negatively correlated with a confidence of 95% over 85% of the domain. Another confirmation of this parity is the shape of the plot of phytoplankton bins versus vorticity bins (figure 6), which displays a pronounced phytoplankton maximum in the negative-vorticity region.

4. Discussion

These numerical results strongly suggest that the LFV of the mesoscale turbulence drives a significant time variability of the spectral characteristics of the plankton distribution and in particular the emergence of more or less energetic small horizontal scales. A signature of this dynamical guidance is the relation in physical space

between dynamical and biological variables, and particularly the good anticorrelation between vorticity and phytoplankton. One may wonder how to explain this anticorrelation over such a large range of spatial scales.

To answer this question, one key point to take into account is that the whole biological system is forced by the vertical advection. This remark allows us to make use of one of the results presented in Klein *et al.* (1998). Interestingly, Klein *et al.* (1998) found that a tracer forced by a large-scale negative vertical gradient is strongly anticorrelated with the potential vorticity. Since the relative vorticity in the surface layers is very close to the potential vorticity, and since nitrate distribution is characterized by a strong negative vertical gradient, the dynamical arguments developed in Klein *et al.* (1998) are certainly pertinent in explaining the strong anticorrelation (-0.73) found in this study between vorticity and nitrate below the euphotic zone (which drives the anticorrelation between vorticity and phytoplankton, since nitrate is rapidly transformed into phytoplankton within the euphotic layer). In Klein *et al.* (1998), the dynamical characteristics of the mesoscale eddy field are set up (as here) by both a large-scale vertical density gradient (the so-called stratification) and a large-scale horizontal density gradient (which makes the flow to be baroclinically unstable). During the nonlinear equilibration period, the physical system, to prevent a thermal-wind imbalance (which would produce dynamical inconsistency), *locally organizes* the vertical and horizontal velocity fields such that vertical and horizontal advection of densities tend to compensate each other. This phase relationship between vertical and horizontal advection (which also suggests that motions are almost parallel to the isopycnals) explains that very few small-scale features are present in the density field, leading to a steep slope of the density spectrum. This compensation between horizontal and vertical advection holds for any tracer forced by the same large-scale vertical *and* horizontal gradients, but not for a tracer forced by either the horizontal *or* the vertical gradient. In the last two cases, small scales will develop, and the consequence of the phase relationship is that a tracer forced by a large-scale horizontal gradient will have its small scales strongly anticorrelated to those of a tracer forced by a large-scale vertical gradient. To restate this argument (see Klein *et al.* 1998 for details) more simply, motions (almost parallel to the isopycnals) are not an efficient mechanism for increasing density gradients, but are efficient enough to increase the gradients of properties whose isopleths are inclined to the isopycnals. Vorticity and nitrate have their isopleths almost orthogonal (and therefore both inclined to the isopycnals), since vorticity is forced by a large-scale horizontal gradient and nitrate by a large-scale vertical gradient. This explains why small scales of vorticity should be strongly anticorrelated to those of nitrate, and ultimately to those of phytoplankton, although a more thorough study is required to understand the additional contribution of the physics linked to the frontogenesis processes (not taken into account in Klein *et al.* (1998)). The results of Klein *et al.* (1998) also suggest another situation that is worth mentioning: since a tracer only forced by a large-scale horizontal gradient should be strongly correlated with the potential vorticity, we can reasonably assume that the findings obtained in the present study should be similar (but strongly anticorrelated) to those from a situation where plankton patchiness is forced by a large-scale nutrient injection involving a large-scale horizontal gradient (i.e. not far from that described by Abraham (1998)).

A simpler (but less-physical and less-accurate) explanation of the strong anticorrelation between vorticity and plankton would invoke the equation for the relative

vorticity integrated in the surface layers: this equation is similar to that of a passive tracer (as nutrients) forced by vertical advection, except for the sign of vertical velocity. The plots of the 'averaged values' of phytoplankton against those of the relative vorticity, as well as those of the vertical velocity against those of the relative vorticity (figure 6), appear to confirm the preceding arguments.

5. Conclusion

The question addressed in this study was: does the LFV inherent to mesoscale turbulence explain a part of the spectral variability of plankton patchiness? The answer provided by the results of our simple experiments is positive. The physics displays a significant LFV (30–100 days) both in terms of the EKE (including the vertical velocity variance) and of the spectral characteristics (i.e. the spatial distribution) of temperature and vorticity. The same LFV characterizes the spatial heterogeneity of the biological variables. Furthermore, a significant phase relationship has been found between the plankton spatial distribution and that of the relative vorticity. The spatial correlation between the physical and biological variables confirms the dominant role of the physics in setting up the spatial variability of plankton distribution. The mechanisms in this study are more complex than those of previous studies, since they involve nutrient input by the vertical pumping *organized* by the eddy field instead of a large-scale vertical injection (Abraham 1998) or small-scale spots of vertical injection with no precise phase relationship with the eddy field (Martin *et al.* 2002). It is expected that the answer given by the results of the present study will still hold in the real world. They *do not* rule out the role of biological factors on the phytoplankton and zooplankton spatial distributions. They suggest that this role can be assessed only when the part of LFV of the mesoscale eddy field is well estimated and removed.

Anne-Marie Tréguier is thanked for fruitful discussions. The OPA system team has made this work possible by maintenance of the OPA tracer code. Simulations were performed on the NEC-SX5 of the IDRIS centre. SAXO (developed by S. Masson) has been a great help in producing the graphics. Funding for this study was provided by the French Ministère de la Recherche (through the ACI programme) and the CNRS (through the PROOF programme).

Appendix A. The numerical simulations

The primitive equation model OPA is used together with an embedded-ecosystem model (see Lévy *et al.* 2001*a*) comprising six state variables (phytoplankton, zooplankton, nitrate, ammonium, dissolved organic matter and detritus). The domain geometry is a flat, zonally periodic channel on a β plane, closed at the north and south boundaries, $960 \times 1300 \times 4\,\mathrm{km}^3$ centred at 35 °N. For the sake of simplicity, a linear equation of state is assumed (see Lévy *et al.* 2001*a*). The initial state is a uniform meridional density gradient in hydrostatic and geostrophic balance. The horizontal density gradient covers a region of *ca.* 600 km width, and gives rise to a weak eastward flow with maximum velocities of $0.1\,\mathrm{m\,s}^{-1}$ at the surface. The mean density profile yields a first baroclinic Rossby radius of deformation (that characterizes the scale of the mesoscale structures) of 30 km. The horizontal resolution is 6 km. There are 30 z-coordinate vertical layers, whose thicknesses vary from 10 to 20 m in the upper 100 m, and increase up to 300 m at the bottom. No wind nor net

surface heat forcing is accounted for. Energy is permanently injected into the system on a large scale in the form of available potential energy. This is done by restoring density towards its initial frontal distribution. This density-forcing term takes the form $\gamma \times (\rho(x, y, z, t) - \bar{\rho}(y, z))$, where $\rho(x, y, z, t)$ is the *in situ* density and $\bar{\rho}(y, z)$ is the initial density distribution. γ is set equal to 300 days^{-1}, which corresponds to the life time of the longest-lived eddies and is long relative to the time-scales of plankton. This restoring can be seen as the effect of a large-scale circulation that would maintain the large-scale density gradients on long time-scales. Free-slip conditions and no heat flux are applied along solid boundaries, except at the bottom where a linear friction drag is applied (equal to 4.6×10^{-4} m s^{-1}). Vertical eddy coefficients are computed from an embedded 1.5 turbulent closure model. Horizontal mixing of density and momentum is included through biharmonic friction terms, with a dissipation coefficient $|K| = 10^9$ m^4 s^{-1}. The time-step is 16 min.

We have found in a previous modelling study (Lévy *et al.* 2001*a*) that increasing the numerical resolution from 6 km to 2 km significantly modifies the dynamical fields. This previous study investigated a much more energetic regime. The dissipation coefficients associated with the 2 km and 6 km resolutions were $|K_{2\ \mathrm{km}}| = 0.5 \times 10^9$ m^4 s^{-1} and $|K_{6\ \mathrm{km}}| = 35 \times 10^9$ m^4 s^{-1}. Therefore, in terms of dissipation, the regime of this study is closer (although slightly more dissipative) to the regime of the 2 km experiment of Lévy *et al.* (2001*a*) than to that of the 6 km experiment. We may therefore expect to capture some aspects of the sub-mesoscale frontal dynamics with a horizontal resolution of 6 km, which was not the case for the more energetic experiments of Lévy *et al.* (2001*a*). However, better representation of this small-scale dynamics would definitely require higher horizontal resolution. This was affordable in the case of the Lévy *et al.* (2001*a*) experiments, which lasted for only 25 days and concerned a much smaller domain. It would require enormous computer resources in the present case.

The dynamical model is spun-up for 1600 days before the biological model is activated for another 500 days. The initial conditions for the ecosystem are taken from a 1D configuration where only weak vertical diffusion is taken into account. The 1D configuration is run until an equilibrated oligotrophic situation is reached. In this equilibrated solution, the nitracline, phytoplankton and zooplankton subsurface maxima are located at 110 m depth. This 1D solution is extended to the whole domain, and is used as the initial condition for the 3D simulation. In the 3D solution, plankton maxima remain at the sub-surface, and, as expected for such a regime, at a depth that varies with the intensity of the nitrate injection. Therefore, in order to focus on the horizontal patchiness, we perform our analysis on vertically integrated plankton fields over the top 150 m.

Although it is preferable to use advection schemes that are positive and that minimize dispersion for the transport of biological tracers at mesoscales (Lévy *et al.* 2001*b*), the centred advection scheme is used. This choice is made in order to use the same numerics for the advection and diffusion of momentum, temperature and biological tracers. By this we expect to minimize numerical artefacts in the comparison between temperature, relative vorticity and phytoplankton variance spectra. Centred advection causes the generation of negative tracer values. Negative values are left negative, but are seen as zero for the computation of source–sink terms. The full dynamical-ecosystem simulation is carried out for 500 days. Model outputs are instantaneous fields (snapshots) and have been saved every 10 days.

References

Abraham, E. R. 1998 The generation of plankton patchiness by turbulent stirring. *Nature* **391**, 577–580.

Abraham, E. R. & Bowen, M. M. 2002 Chaotic stirring by a mesoscale surface oceanic flow. *Chaos* **12**, 373–381.

Abraham, E. R., Law, C. S., Boyd, P. W., Lavender, S. J., Maldonado, M. T. & Bowie, A. R. 2000 Importance of stirring in the development of an iron-fertilized phytoplankton bloom. *Nature* **407**, 727–730.

Fasham, M. J. R., Ducklow, H. W. & McKelvie, S. M. 1990 A nitrogen-based model of plankton dynamics in the oceanic mixed-layer. *J. Mar. Res.* **48**, 591–639.

Foujols, M.-A., Lévy, M., Aumont, O. & Madec, G. 2000 *OPA 8.1 Tracer model reference manual*. Note Technique du Pôle de Modélisation du Climat. Paris, France: Institut Pierre Simone Laplace (IPSL). (Available at http://www.ipsl.jussieu.fr).

Ghil, M. & Childress, S. 1987 *Topics in geophysical fluid dynamics: atmospheric dynamics, dynamo theory and climate dynamics*, p. 485. Springer.

Gower, J. F. R., Denman, K. L. & Holyer, R. L. 1980 Phytoplankton patchiness indicates the uctuations spectrum of mesoscale oceanic structure. *Nature* **288**, 157–159.

Held, I. M., Pierrehumbert, R. T., Garner, S. T. & Swanson, K. L. 1995 Surface quasi-geostrophic dynamics. *J. Fluid Mech.* **282**, 1–20.

Klein, P. & Hua, L. 1990 The mesoscale variability of the sea-surface temperature. An analytical and numerical model. *J. Mar. Res.* **48**, 729–763.

Klein, P., Tréguier, A.-M. & Hua, B. L. 1998 Three-dimensional stirring of thermohaline fronts. *J. Mar. Res.* **56**, 589–612.

Kraichnan, R. 1974 Convection of a passive scalar by a quasi-uniform random straining field. *J. Fluid Mech.* **64**, 737–756.

Lapeyre, G., Klein, P. & Hua, B. L. 1999 Do tracer gradient vectors align with strain vectors in 2D flows? *Phys. Fluids* **11**, 3729–3737.

Lévy, M., Klein, P. & Tréguier, A.-M. 2001*a* Impacts of sub-mesoscale physics on phytoplankton production and subduction. *J. Mar. Res.* **59**, 535–565.

Lévy, M., Estublier, A. & Madec, G. 2001*b* Choice of an advection scheme for biogeochemical models. *Geophys. Res. Lett.* **28**, 3725–3728.

Madec, G., Delecluse, P., Imbard, M. & Lévy, C. 1998 *OPA 8.1 Ocean general circulation model reference manual*. Note du Pôle de Modélisation du Climat. Paris, France: Institut Pierre Simone Laplace (IPSL). (Available at http://www.ipsl.jussieu.fr).

Mahadevan, A. & Campbell, J. W. 2002 Biogeochemical patchiness at the sea surface. *Geophys. Res. Lett.* **29**, 1926–1929.

Martin, A. P. & Srokosz, M. A. 2002 Plankton distribution spectra: inter-size class variability and the relative slopes for phytoplankton and zooplankton. *Geophys. Res. Lett.* **29**, 2213–2216.

Martin, A. P., Richards, K. J., Bracco, A. & Provenzale, A. 2002 Patchy productivity in the open ocean. *Global Biogeochem. Cycles* **16**, No. 2, 10.1029/2001GB001449.

Panetta, R. L. 1993 Zonal jets in wide baroclinically unstable regions: persistence and scale selection. *J. Atmos. Sci.* **50**, 2073–2106.

Pedlosky, J. & Frenzen, C. 1980 Chaotic and periodic behavior of finite-amplitude baroclinic waves. *J. Atmos. Sci.* **37**, 1177–1196.

Penduff, T., Barnier, B., Dewar, W. K. & Brien, J. J. O. 2004 Impact of the North Atlantic Oscillation on the oceanic eddy flow: dynamical insights from a model-data comparison. *J. Phys. Oceanogr.* (In the press.)

Powell, T. M. & Okubo, A. 1994 Turbulence, diffusion and patchiness in the sea. *Phil. Trans. R. Soc. Lond.* B **343**, 11–18.

Smith, K. S. & Vallis, G. K. 2001 The scales and equilibration of midocean eddies: freely evolving flow. *J. Phys. Oceanogr.* **31**, 554–571.

Smith, R. C., Zhang, X. & Michaelsen, J. 1988 Variability of pigment biomass in the California current system as determined by satellite imagery. 1. Spatial variability. *J. Geophys. Res.* **93**, 10 863–10 882.

Smith, C. L., Richards, K. J. & Fasham, M. J. R. 1996 The impact of mesoscale eddies on phytoplankton dynamics in the upper ocean. *Deep-Sea Res. I* **43**, 1807–1832.

Stammer, D. 1997 Global characteristics of ocean variability estimated from regional TOPEX/ Poseidon altimeter measurements. *J. Phys. Oceanogr.* **27**, 1743–1769.

Stammer, D. & Wunsch, C. 1999 Temporal changes in eddy energy of the oceans. *Deep-Sea Res. II* **46**, 77–108.

Strutton, P. G., Mitchell, J. G., Parslow, J. S. & Greene, R. M. 1997 Phytoplankton patchiness: quantifying the biological contribution using fast repetition fluorometry. *J. Plankton Res.* **19**, 1265–1274.

Tennekes, H. & Lumley, J. L. 1972 *A first course in turbulence*, p. 300. Cambridge, MA: MIT Press.

Tréguier, A. M. & Panetta, R. L. 1994 Multiple zonal jets in a quasi-geostrophic model of the antarctic circumpolar current. *J. Phys. Oceanogr.* **24**, 2263–2277.

Vautard, R. & Legras, B. 1988 On the source of mid-latitude low-frequency variability. II. Nonlinear equilibration of weather regimes. *J. Atmos. Sci.* **45**, 2845–2867.

Washburn, L., Emery, B. M., Jones, B. H. & Ondercin, D. G. 1998 Eddy stirring and phytoplankton patchiness in the subarctic North Atlantic in late summer. *Deep-Sea Res. I* **45**, 1411–1439.

Wunsch, C. 1997 The vertical partition of oceanic horizontal kinetic energy. *J. Phys. Oceanogr.* **27**, 1770–1794.

Yoder, J. A., Aiken, J., Swift, R. N., Hoge, F. E. & Stegmann, P. M. 1993 Spatial variability in near-surface chlorophyll a fluorescence measured by the airborne oceanographic lidar (AOL). *Deep-Sea Res. II* **40**, 37–53.